

Article

Using Factor Analysis to Determine the Interrelationships between the Engineering Properties of Aggregates from Igneous Rocks in Greece

Panagiota P. Giannakopoulou ^{1,*}, Petros Petrounias ¹ , Basilios Tsikouras ² , Stavros Kalaitzidis ¹ , Aikaterini Rogkala ¹, Konstantin Hatzipanagiotou ¹ and Stylianos F. Tombros ¹

¹ Section of Earth Materials, Department of Geology, University of Patras, 265 04 Patras, Greece; Geo.plan@outlook.com (P.P.); skalait@upatras.gr (S.K.); krogkala@upatras.gr (A.R.); k.hatzipanagiotou@upatras.gr (K.H.); tombrosfs@gmail.com (S.F.T.)

² Physical and Geological Sciences, Faculty of Science, Universiti Brunei Darussalam, Jalan Tungku Link, Gadong BE1410, Brunei Darussalam; basilios.tsikouras@ubd.edu.bn

* Correspondence: peny_giannakopoulou@windowslive.com

Received: 7 November 2018; Accepted: 6 December 2018; Published: 8 December 2018



Abstract: This paper investigates the interrelationships between the engineering properties of igneous aggregate rocks from Greece with the aid of the R-mode factor analysis. The collected samples represent mafic and ultramafic rocks from the ophiolite complexes of Gerania, Guevgueli, Veria-Naousa, and Edessa as well as intermediate-acidic rocks from the surrounding areas of the complexes. Factor analysis verifies the important interdependences among the engineering parameters like physical, mechanical, geometrical, and physicochemical properties by giving statistical significance. Variations of the petrographic characteristics of the investigated rocks influence their engineering properties as well as the interdependence among them. Factor 1, which is the most representative one (~36% of the total variance), shows interdependences between certain physical, mechanical, physicochemical properties such as total porosity (n_t) with moisture content (w), n_t with the Los Abrasion value (LA), and the uniaxial compressive strength (UCS) with point load index $Is_{(50)}$. Additionally, the second factor (~27% of the total data variability) correlates physical properties such as w , n_t , physicochemical properties such as the methylene blue test (MB_F), mechanical properties such as UCS, $Is_{(50)}$, and loss on ignition (LOI), which highlights the effect of mineralogy on these properties. Lastly, Factor 3 (~14% of the total data variability) expresses the interdependence of the flakiness index (I_F), which is an elongation index (I_E) relative to their alteration (LOI).

Keywords: engineering properties; petrographic features; igneous aggregate rocks; factor analysis; construction materials

1. Introduction

Aggregates with distinguishable different origins are widely utilized for a variety of construction applications especially as a road stone, railway ballasts, and some concrete applications. An enormous amount of aggregate is used annually worldwide. Currently, the demand of crushed stone aggregates increases because of the increasing expansion of highway and other construction projects and the decreasing availability of global natural aggregate resources. Different types of rocks have different impacts on construction. The quality of aggregates is of considerable significance in determining their suitability for any engineering application [1].

Igneous rocks are commonly hard and dense, which results in an excellent source of aggregate materials. However, certain extrusive rocks are too porous to be used as aggregates while some highly siliceous igneous rocks tend to chemically react with alkali when they are used as concrete aggregates. Fractures in some rocks may render them unsuitable for aggregate use. Similarly, some lava-flow rocks are considered unsuitable for aggregates. When they contain flow banding, they are strongly jointed or brecciated. Furthermore, pyroclastic volcanic materials such as ash and tuff may be unsuitable unless they have become indurated by heating or compacted and cemented during burial.

The study of the engineering properties of rock materials as well as their respective mineralogical and textural characteristics decisively determines the rock's strength and its capability from failure [2–12]. The engineering parameters of igneous rocks are controlled by several inherent and environmental parameters while one of the most significant parameters is the alteration. The inherent parameters can be determined by their petrographical properties, which control the engineering properties of igneous rocks. Many studies have been concentrated on granitic rocks [13,14]. However, several authors have conducted analogous studies in acidic-intermediate volcanic rocks [15,16], metamorphic rocks [17,18], and mafic [5,19] and ultramafic rocks [11,12,19–21]. Alteration is a critical factor as increased percentages of certain secondary minerals such as serpentine and talc affect negatively the mechanical properties of ultramafic aggregates due to their layered structure, cleavage, and platy or fibrous crystal habit [11,20]. Chlorite is a common secondary mineral in mafic rocks and it is known to have a critical effect on the freeze-thaw durability of the aggregates in concrete. Clay minerals are common secondary minerals in intermediate-acidic rocks such as andesites and dacites.

The prediction of one engineering parameter through the other is an important field of research. Kazi and Al-Mansour [22] obtained strong correlations between uniaxial compressive strength, Schmidt hammer, and Los Angeles abrasion after testing volcanic and plutonic rocks. Chargill and Shakoor [23] established a non-linear inverse relation between the compressive strength and LA abrasion after testing sedimentary and metamorphic rocks. Christensen [24] focused on the relationship between the mechanical strength of serpentinized rocks with their physical and mechanical properties. Kahraman [25] studying a variety of igneous, sedimentary, and metamorphic rocks has reported good correlations between the uniaxial compressive strength and the LA abrasion. He has also mentioned that, when these rocks are classified into classes of porosity, the correlation coefficients increase. Ugur et al. [26] have also pointed out high correlations between the LA abrasion and the compressive strength, Schmidt hardness, and the point load index in a variety of aggregate rocks. Giannakopoulou et al. [9] mentioned inverse relationships between the point load index, the compressive strength, and the LA abrasion for ultramafic aggregate rocks.

The most common statistical method used to correlate geological data and more specifically engineering properties of aggregate rocks is regression analysis [2,8,9,11,12,20,27]. Some researchers have noticed the importance of other statistical methods such as factor analysis and Q-mode analysis in a wide range of geological subjects [28–31]. Factor analysis is a multivariate, well-known statistical technique, which uses uncorrelated variables called factors and explain the variance observed in the original dataset [32,33]. This technique has been successfully applied in hydrochemistry [34,35], geochemistry [36–40], and less in engineering geology [41,42].

The goal of this study is to investigate the interrelationships between the engineering parameters of igneous rocks derived from various localities in Greece (Figure 1) using factor analysis. In order to export when more representative results could be exported, a wide range of igneous lithotypes were collected and studied, characterized by a great variety of engineering properties, and of petrographic features, which enhances the suggestions of previous researchers by the interaction of the engineering parameters for having as much statistical significance as possible.

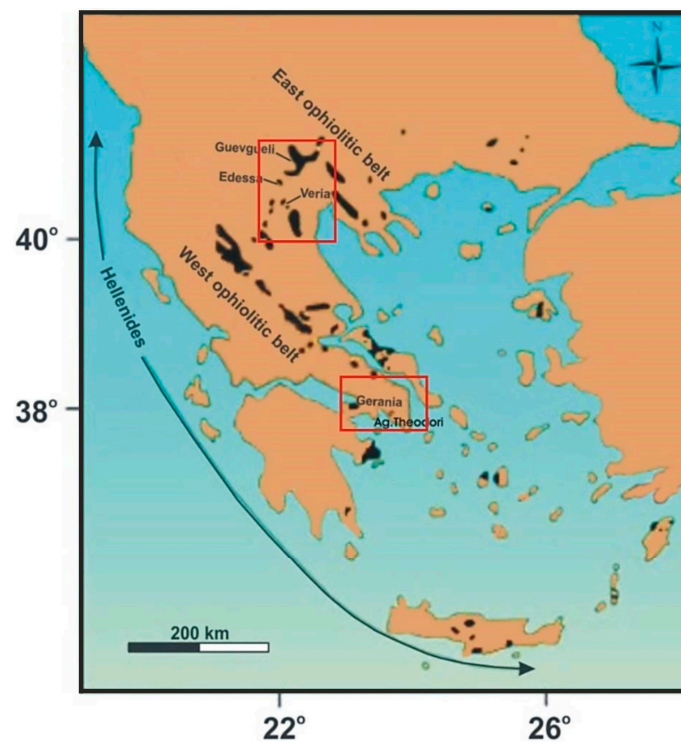


Figure 1. Simplified map showing the sampling areas in the red rectangles.

2. Geological Setting

The Veria-Naousa ophiolite complex, which is located in Northern Greece, belongs to the Almopias subzone of the Axios geotectonic zone. This complex consists of, from the base to the top, intensely tectonized and serpentized lherzolite and harzburgite crosscut by few pyroxenitic dykes, gabbro, diabase, and pillow basalt [43]. The Upper Jurassic to Lower Cretaceous Edessa ophiolite comprises several tectonic units and includes lherzolite, highly serpentized harzburgite, diorite, metamorphic gabbro, diabase, and basalt [44–46]. The incomplete and dismembered Gerania ophiolite complex belongs to the Pelagonian geotectonic zone and consists of variably altered harzburgite, lherzolite, and dunite [47–49]. Gabbro dikes interrupt the serpentized peridotites. The Middle-Late Jurassic Guevgueli Complex of the Vardar Zone is sub-divided into two distinct sub-units, which are the East and the West Guevgueli and both include intrusive and volcanic sequences crosscut by several dykes. This complex is intruded by the Fanos Granite and, with this together, is sandwiched through an N-trending striking thrust zone between the Serbomacedonian Massif to the east and the Paikon Unit to the west. Both the West and East Guevgueli include olivine gabbro, amphibole gabbro, diorite, and diabase [50,51]. Pliocene intermediate to acidic volcanic rocks occur to the east of the Edessa ophiolite and they belong to the Almopias subzone [52,53]. The Ag. Theodoroi volcanic rocks, derived from the Crommyonia mark of the western end of the south Aegean volcanic arc include outcrops of Pliocene dacites, which appear spatially related to extensional faults at the margin of the Saronicos basin [54].

3. Materials and Methods

In order to investigate the petrographic characteristics and the engineering properties of the aggregate rocks, ultramafic, mafic, and intermediate-acidic aggregate blocks were collected from quarries and other outcrops from the studied areas, according to the EN 932-1 [55] standard. The samples were subsequently prepared in order to be suitable for all the engineering tests, which were performed according to European and International standards.

The petrographic features of the studied samples were examined in thin sections using a polarizing microscope (Leica Microsystems Leitz Wetzlar, Germany), according to the EN-932-3 [56] standard for a petrographic description of aggregates. The mineralogical composition of the studied samples was also determined with X-ray Diffraction, according to EN-932-3 [56] using a Bruker D8 advance diffractometer with an Ni-filtered $\text{CuK}\alpha$ radiation. Random powder mounts were prepared by gently pressing the powder into the cavity holder. The scanning area for bulk mineralogy of specimens covered the 2θ interval $2\text{--}70^\circ$ with a scanning angle step size of 0.015° and a time step of 0.1 s. The mineral phases were determined by using the DIFFRACplus EVA 12[®] software (Bruker-AXS, GmbH, Karlsruhe, Germany) based on the ICDD Powder Diffraction File of PDF-2 2006.

The determined physical properties are the moisture content [57], total porosity, and dry density [58]. Geometrical properties included the flakiness index (I_F) [59] and the elongation index (I_E) [60]. The studied samples have been crushed in a laboratory-jagged crusher. The mechanical properties of the Los Angeles abrasion value (LA), uniaxial compressive strength (UCS), the point load index ($I_{s(50)}$), and the Schmidt hammer value (SHV) were also determined. The Los Angeles abrasion (LA) test measures the resistance of aggregates to abrasion, attrition, and grinding, which indicates that the lower LA abrasion values of rocks correspond to more resistant rocks in abrasion and attrition. This test was carried out in accordance to the ASTM C-131 [61] standard using the “B” gradation. The uniaxial compressive strength (UCS) is one of the most significant engineering properties of rocks. The UCS test was carried out in six cylindrical rock specimens with height/diameter ratios between 2 and 3. Their diameters range from 51 to 54 mm (ASTM D-2938 [62]) and the average values were used for each set of specimens. The point load index ($I_{s(50)}$) is used in order to obtain an indirect measure of the uniaxial compressive strength, according to the ISRM [63] standard. The Schmidt hammer test is a non-destructive method to characterize the rock hardness and strength. The test was carried out using the L type Schmidt hammer on cylindrical specimens [58]. The physicochemical properties, which were calculated for this study is the Soundness test (S) [64] and the methylene blue test (MB_F) [65]. The soundness test is used for the assessment of the ability to resist the aggregates in the excessive volume changes relative to the changes in the physical environment. The MB_F is an indirect method for determining the swelling clay minerals in the aggregate rocks. This test was determined on the aggregate fraction of 0–0.125 mm. Furthermore, loss on ignition (LOI) in all samples was determined according to the ASTM D7348-13 standard [66].

4. Results

4.1. Petrographic Features

According to the EN 932-1 [55] standard, the comprehensive petrographic characterization was achieved by: (i) microscopic observation of polished-thin sections of the samples under a polarizing microscope and (ii) the X-ray Diffractometry of powdered specimens.

4.1.1. Ultramafic Rocks

The studied ultramafic rock samples are comprised of dunite, harzburgite, and lherzolite (for specific types and provinces, see Table 1). The peridotites from the Gerania ophiolite show generally lower degrees of serpentinization and deformation relative to those from the Veria-Naousa and Edessa suites. One orthopyroxenite specimen from Veria-Naousa shows a very small degree of alteration.

Dunite presents cataclastic and locally granular textures (Figure 2a). Primary assemblage includes mostly olivine and scarce relics of orthopyroxene. Infrequent chromite is present, too. Serpentine is the dominant secondary phase and some highly serpentinized samples show mesh as well as locally ribbon and interwoven textures. Secondary talc and chlorite occur in minor amounts.

Table 1. Petrographic characteristics of the studied igneous rocks.

No.	Samples	Lithotype	Texture	Primary Minerals	Secondary Minerals
1	GE.4/Gerania	Srp. Harzburgite	Mesh	ol, opx, sp,	srp, act, bas
2	GE.17/Gerania **	Dunite	Granular, cataclastic, mesh, ribbon, interwoven	ol, opx, sp, chr	srp, talc, bruc
3	GE.25/Gerania **	Lherzolite	Granular, porphyroclastic	ol, opx, cpx, sp	srp
4	GE.26/Gerania **	Srp. Lherzolite	cataclastic, porphyroclastic, mesh, ribbon	ol, opx, cpx, sp	srp, talc, bas
5	GE.28/Gerania **	Harzburgite	Granular, cataclastic, porphyroclastic, ribbon	ol, opx, cpx, sp	srp
6	GE.30/Gerania **	Lherzolite	Cataclastic, porphyroclastic, mesh, ribbon	ol, opx, cpx, sp	srp, chl, mgt
7	GE.31/Gerania **	Lherzolite	Cataclastic, porphyroclastic, ribbon	ol, opx, cpx, sp	srp, chl, act, mgt
8	GE.32/Gerania **	Lherzolite	Granular, cataclastic, porphyroclastic, ribbon	ol, opx, cpx, sp	srp, chl, talc, mgt
9	GE.33/Gerania **	Lherzolite	Granular, cataclastic, porphyroclastic, ribbon	ol, opx, cpx, sp	srp, chl, talc, mgt
10	GE.34/Gerania **	Dunite	Granular, cataclastic, porphyroclastic, ribbon	ol, opx, sp, chr	srp, talc, chl
11	GE.35/Gerania	Lherzolite	Granular, cataclastic, porphyroclastic, mesh, ribbon	ol, opx, cpx, sp	srp, chl
12	GE.36/Gerania	Lherzolite	Cataclastic, porphyroclastic, mesh, ribbon	ol, opx, cpx, sp	srp, chl, act
13	GE.37/Gerania **	Dunite	Granular, cataclastic, porphyroclastic, mesh, ribbon	ol, opx, cpx, sp, chr	srp, talc, chl, bas, ath
14	GE.39/Gerania **	Lherzolite	Cataclastic, porphyroclastic, mesh, ribbon	ol, opx, cpx, sp	srp, chl, act
15	BE.01A/Veria	Srp. Harzburgite	Ribbon, mesh, bastite	opx, ol, sp	srp, mgt, bas
16	BE.01B/Veria **	Srp. Harzburgite	Ribbon, mesh, bastite	opx, ol, sp	srp, mgt, bas
17	BE.12/Veria *	Srp. Harzburgite	Ribbon, mesh, bastite	opx, ol, cpx, sp	srp, mgt, bas, grt
18	BE.12B/Veria **	Srp. Harzburgite	Ribbon, mesh, bastite	opx, ol, cpx, sp	srp, mgt, bas, grt
19	BE.67/Veria ****	Pyroxenite	Porphyroclastic, mesh	opx, cpx, ol	srp, chl, talc, tr, mgt
20	BE.103/Veria ***	Srp. Lherzolite	Ribbon, mesh, bastite, interlocking	opx, cpx, sp	srp, chl, mgt
21	BE.103B/Veria **	Srp. Lherzolite	Ribbon, mesh, bastite	opx, ol, cpx, sp	srp, chl, mgt, bas
22	BE.103C/Veria	Srp. Lherzolite	Ribbon, mesh, bastite	opx, ol, cpx, sp	srp, mgt, bas
23	BE.122/Veria **	Srp. Harzburgite	Ribbon, mesh, bastite	opx, ol, cpx, sp	srp, mgt, bas
24	BE.122B/Veria	Srp. Harzburgite	Ribbon, mesh, bastite	opx, ol, sp	srp, mgt, bas
25	BE.133/Veria *	Srp. Lherzolite	Ribbon, mesh, bastite, interlocking	sp	srp, mgt, chl, bas
26	ED.59/Edessa ***	Srp. Harzburgite	Ribbon, mesh, bastite	sp	srp, mgt, bas
27	ED.115/Edessa ***	Srp. Harzburgite	Ribbon, mesh, bastite	sp	srp, mgt, bas
28	BE.77/Veria	Diorite	Granular, ophitic to subophitic	cpx, plg, or, qz	ser, chl, ep, chl, act
29	ED.93/Edessa	Diorite	Granular	plg, hbl, cpx, or, qz, ttn	ser, act, chl, stl
30	ED.94/Edessa	Diorite	Granular	plg, hbl, cpx, or, qz, ttn	ser, act, chl, stl
31	GE.24/Gerania	Troctolite	Granular, cumulate	plg, ol, opx, cpx	ser, act, chl, ep, grt, srp, cc
32	KIL.1/Guevgueli	Hbl-Gabbro	Granular, ophitic, cumulative	plg, cpx, amp	chl, act, ep, ser, tr
33	KIL.4/Guevgueli	Hbl-Gabbro	Granular, subophitic	plg, cpx, amp	chl, act, ep, ser, qz
34	KIL.5/Guevgueli	Hbl-Gabbro	Granular, ophitic	plg, cpx, opx, amp	chl, act, ep, ser
35	KIL.6/Guevgueli	Hbl-Gabbro	Granular, ophitic	plg, cpx, opx, ol, amp	chl, act, ep, ser

Table 1. Cont.

No.	Samples	Lithotype	Texture	Primary Minerals	Secondary Minerals
36	KIL.9/Guevgueli	Qz-Hbl-Gabbro	Ophitic, cumulative	plg, cpx, amp, qz	chl, act, ser, ep
37	KIL.10/Guevgueli	Qz-Hbl-Gabbro	Ophitic, cumulative	plg, cpx, amp, qz	chl, act, ser, ep
38	BE.100/Veria	Gabbro	Granular, ophitic to subophitic	cpx, plg, ttn	chl, act, ep
39	ED.26B/Edessa	Gabbro	Ophitic to subophitic	cpx, plg, ttn	chl, ser, ep, phr
40	KIL.2/Guevgueli ***	Diabase	Subophitic	plg, cpx, opx, amp, ttn	chl, act, ser, ep
41	KIL.3/Guevgueli ***	Diabase	Subophitic	plg, cpx, opx, amp, ttn	chl, act, ser, ep
42	KIL.8/Guevgueli	Diabase	Subophitic	plg, cpx, opx, amp, ttn	chl, act, ser, ep
43	BE.24/Veria	Diabase	Subophitic	plg, cpx, ttn	chl, act, ep
44	BE.43/Veria ***	Diabase	Ophitic, cataclastic	plg, cpx	chl, act, ep
45	ED.24/Edessa ***	Diabase	Subophitic	plg, cpx	act, chl, ep, phr, ser
46	BE.113/Veria	Diabase	Cataclastic	plg, cpx	chl, act, ep
47	ED.45/Edessa	Diabase	Porphyritic, Interlocking	plg, cpx	chl, ep, ser, act
48	ED.66B/Edessa	Diabase	Porphyritic, Interlocking	plg, cpx	chl, ep, ser, act
49	ED.110/Edessa ***	Diabase	Subophitic	plg, cpx	chl, act, ep
50	BE.15/Veria	Basalt	Porphyritic, interwoven	plg, cpx	ep, chl, phr, act
51	ED.66A/Edessa	Basalt	Interwoven, porphyritic	plg, cpx	chl, ep, act
52	GE.22/Ag. Theod ***	Dacite	Porphyritic	plg, hbl, san, or, bi, qz	ser
53	GE23/Ag. Theod ***	Dacite	Porphyritic	plg, hbl, san, or, bi, qz	ser
54	BE.81B/Veria	Andesite	Porphyritic, microlithic	plg, hbl, cpx, san, bi, qz	chl, ser
55	BE.82B/Veria	Andesite	Porphyritic, microlithic	plg, hbl, cpx, san, bi, qz	chl, ser
56	BE.88/Veria *	Andesite	Porphyritic, microlithic	plg, hbl, cpx, san, bi	chl, ser
57	BE.89/Veria *	Andesite	Porphyritic, microlithic, trachytic	plg, hbl, cpx, san, bi	chl, ser
58	BE.101B/Veria	Andesite	Porphyritic, microlithic	plg, hbl, cpx, san, bi, qz	chl, ser
59	BE.139/Veria	Granodiorite	Granular, porphyritic	qz, plg, or, ttn	chl, ep, ser
60	BE.140/Veria	Granodiorite	Granular, porphyritic	qz, plg, or	chl, ep, ser
61	BE.149/Veria	Granodiorite	Granular, porphyritic	qz, plg, or	chl, ep, ser
62	BE.108/Veria	Albitite	Subophitic	plg, cpx, qz	chl, ep, ser
63	BE.150/Veria	Albitite	Subophitic	plg, cpx, qz	chl, ep, ser

(ol = olivine, opx = orthopyroxene, cpx = clinopyroxene, sp = spinel, chr = chromite, act = actinolite, bas = bastite, bruc = brucite, talc = talc, chl = chlorite, mgt = magnetite, grt = garnet, tr = tremolite, ep = epidote, plg = plagioclase, or = orthoclase, qz = quartz, ath = anthophyllite, hbl = hornblende, stl = stilpnomelane, ttn = titanite, ser = sericite, cc = calcite, amp = amphibole, phr = prehnite, san = sanidine, bi = biotite, srp = serpentine; * = previously published samples by Petrounias et al. [10], ** = previously published by Giannakopoulou et al. [12], *** = previously published by Petrounias et al. [11], and **** = previously published by Rogkala et al. [42]).

Harzburgite presents porphyroclastic and locally cataclastic texture. Its primary assemblage includes olivine, orthopyroxene, and rare clinopyroxene. Olivine appears as porphyroclasts, which present strong deformation as well as small-sized unstrained neoblasts. Al-spinel and Cr-spinel are present in small amounts including some that display embayed margins and rims altered to a secondary magnetite. A dense network of microcracks also occurs. The serpentine comprises the most common secondary phase presenting mesh, bastitic, cataclastic, and ribbon texture. Chlorite is also present (Figure 2b). Brittle deformation is expressed by intense fragmentation of the spinel as well as by intragranular microcracks.

Lherzolite shows protogranular, porphyroclastic, and locally cataclastic textures with the primary assemblage including olivine, orthopyroxene, and clinopyroxene (Figure 2c). Al-spinel is present in small amounts. Serpentine is the main secondary mineral, which shows mostly mesh, bastitic, cataclastic, and locally ribbon textures. Other secondary phases are chlorite and actinolite. A dense network of microcracks is also observed in lherzolite.

Orthopyroxenite is the least altered lithology and generally presents coarse, granular, and porphyroclastic texture. It consists mainly of orthopyroxene, rare clinopyroxene, olivine, and spinel. Orthopyroxenes exhibit intense ductile deformation, undulatory extinction, and frequent exsolution lamellae of clinopyroxene (Figure 2d).

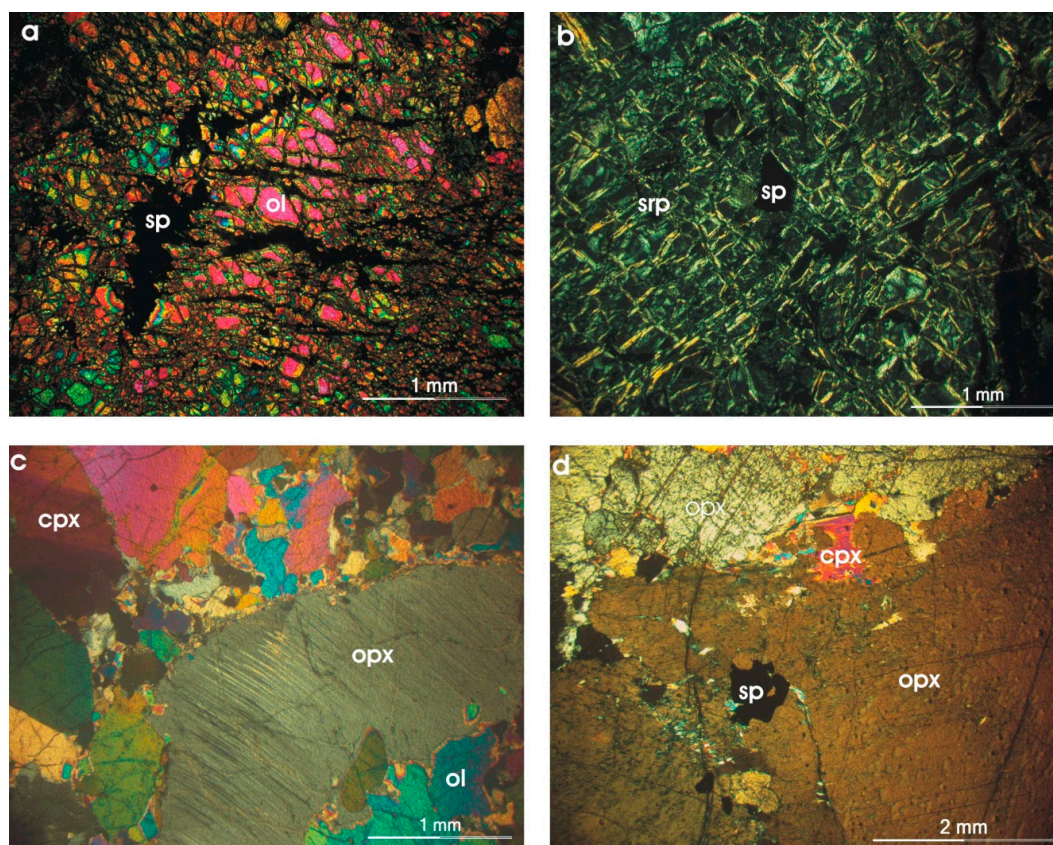


Figure 2. Photomicrographs of representative ultramafic aggregate rocks (XPL): (a) cataclastic olivine in a dunite (sample GE.34). (b) mesh serpentine and crystals of spinel in a serpentinized harzburgite (sample BE.01). (c) porphyroclasts of orthopyroxene showing kink banding, olivine, and clinopyroxene in a porphyroclastic lherzolite (sample GE.30). (d) porphyroclasts of orthopyroxene in pyroxenite and scarce crystals of spinels (sample BE.67). Abbreviations: ol: olivine, sp: spinel, srp: serpentine, opx: orthopyroxene, cpx: clinopyroxene.

The mineralogical assemblage of the rocks was also identified with the aid of X-Ray diffraction. The X-ray diffraction enabled us to identify the crystalline phases of the studied rocks. Representative

XRD patterns of the samples are shown in Figure 3. The main secondary phases of the ultramafic rocks are serpentine (lizardite), talc, anthophyllite, and magnetite.

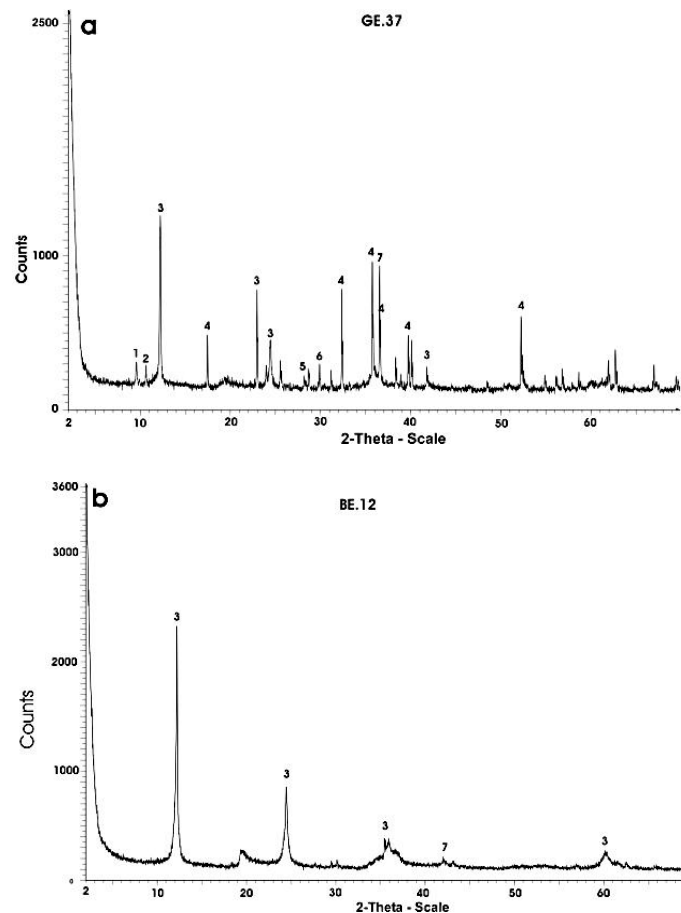


Figure 3. Representative X-ray diffraction patterns of the studied ultramafic rock samples: (a) dunitite and (b) serpentinized harzburgite. Sample numbers are indicated as insets (1: talc, 2: anthophyllite, 3: lizardite, 4: olivine, 5: orthopyroxene, 6: magnetite, 7: spinel).

4.1.2. Mafic Rocks

The studied mafic rock samples include gabbros and diabases from the Guevgueli, Veria-Naousa, and Edessa ophiolite suites, troctolite from the Gerania ophiolite, and diorites and basalts from the Veria-Naousa and Edessa ophiolites (Table 1).

Gabbros derived from the Guevgueli and the Veria-Naousa ophiolite complexes exhibit granular, ophitic, and locally porphyritic textures with subhedral to euhedral plagioclase phenocrysts (Figure 4a). The primary assemblage of gabbro consists of clinopyroxene (mainly diopside), plagioclase, amphibole (the last only in Guevgueli), and local olivine. Chlorite, actinolite, and epidote are secondary minerals while ilmenite, titanite, and magnetite constitute accessory phases. The most altered gabbro from the Edessa ophiolite complex consists only of clinopyroxene since plagioclase has been nearly eliminated. This rock exhibits a high percentage of chlorite with coarse crystals, which are unevenly distributed in the sample. Primary textures have been obliterated by deformation.

Troctolite exhibits granular and cumulate textures. Its primary assemblage consists of olivine, orthopyroxene, clinopyroxene, plagioclase, and opaque minerals. Chlorite, epidote, serpentine, and garnet are the secondary minerals.

Diabases exhibit porphyritic, ophitic, and subophitic textures (Figure 4b). Their primary assemblages include clinopyroxene and subhedral plagioclase. In some cases, the plagioclase is partially to completely altered to sericite. Ilmenite, magnetite, titanite, and zircon are present as accessory minerals. Chlorite,

actinolite, epidote, and prehnite are secondary phases. Chlorite shows uniform distribution in the diabases and fills up the interstices of the subophitic texture. It should be noted that diabase from the Guevgueli ophiolite is less altered in contrast to those derived from the other ophiolite complexes, which are characterized by higher and variable degrees of alteration.

Diorites are moderately altered and they exhibit a granular texture with subhedral to euhedral plagioclase phenocrysts (Figure 4c). Sporadic, euhedral hornblende grains are poikilitically enclosed within larger plagioclase crystals. Primary assemblages include clinopyroxene, plagioclase, and hornblende. Minor magnetite and ilmenite are also present. Ocean-floor metamorphism resulted in the development of chlorite, actinolite, sericite, albite, epidote, and stilpnomelane. Additionally, quartz fills transgranular microcracks crosscutting the rock.

Basalts display interwoven, porphyritic, and microlitic textures (Figure 4d). Their primary assemblage includes plagioclase, clinopyroxene, magnetite, ilmenite, and accessory zircon. They have suffered a low-grade, oceanic metamorphic episode with the development of quartz, epidote, chlorite, pumpellyite, actinolite, calcite, hematite, and titanite, which occurs in the groundmass and within joints or amygdules. The matrix is glassy with fine plagioclase crystals.

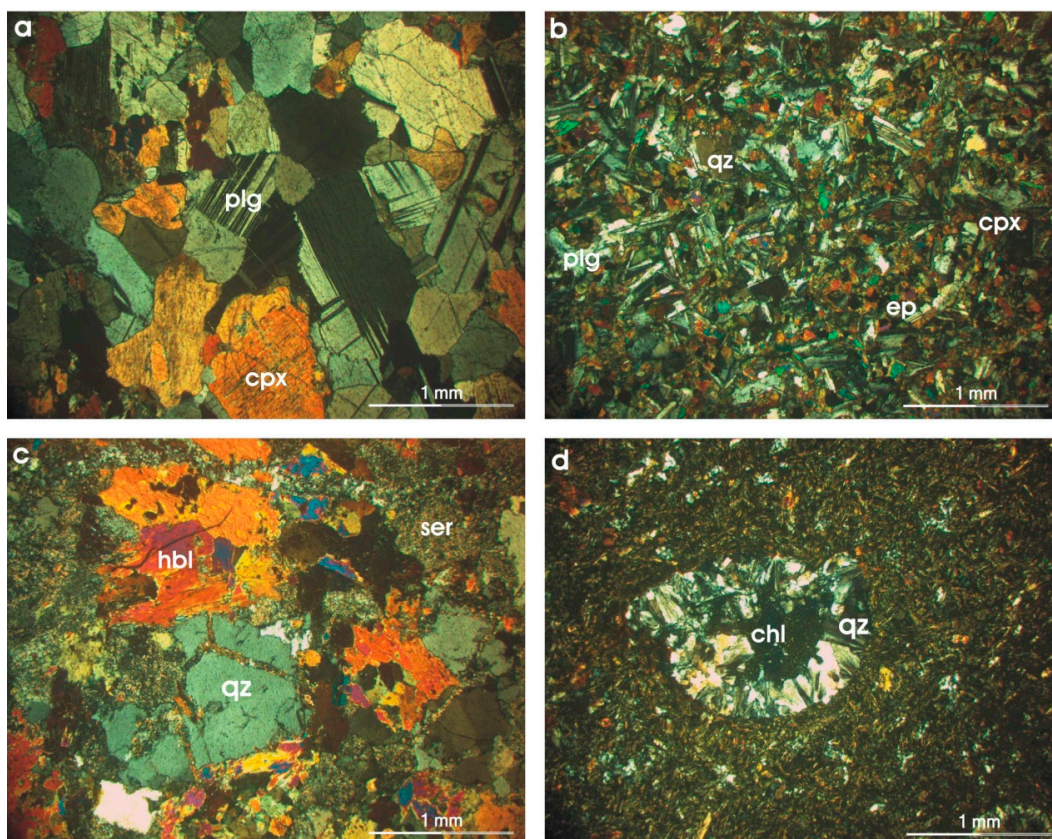


Figure 4. Photomicrographs of representative mafic aggregate rocks (XPL): (a) granular subhedral texture in a gabbro (sample KIL.5), (b) subophitic texture in a diabase with crystals of quartz and epidote (sample KIL.3), (c) granular with subhedral to euhedral intensely altered plagioclase as well as hornblende and quartz in a diorite (sample BE.77), and (d) porphyritic and microlitic textures in basalt with amygdules containing chlorite surrounded by quartz (sample ED.66A). Abbreviations: plg: plagioclase, qz: quartz, cpx: clinopyroxene, ep: epidote, hbl: hornblende, ser: sericite, chl: chlorite.

The petrographic observation by X-ray diffraction patterns showed that the secondary phases of the studied mafic rocks are chlorite, actinolite, and epidote (Figure 5).

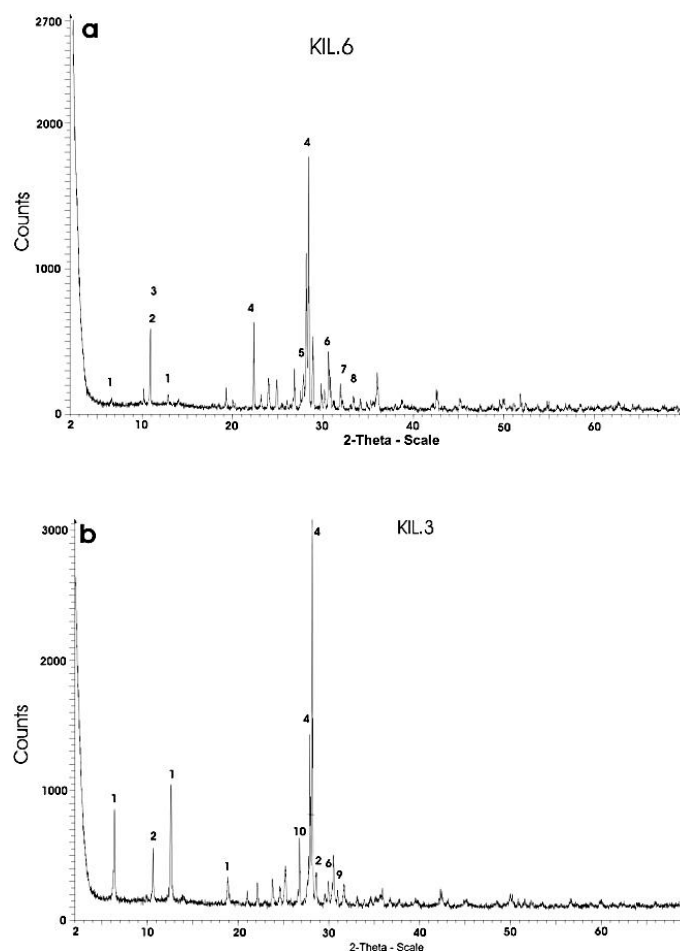


Figure 5. Representative X-ray diffraction patterns of the studied mafic rock samples: (a) gabbro and (b) diabase. Sample numbers are indicated as insets (1: chlorite, 2: actinolite, 3: hornblende, 4: plagioclase, 5: titanite, 6: orthopyroxene, 7: olivine, 8: apatite, 9: epidote, 10: quartz).

4.1.3. Acidic-Intermediate Rocks

The studied intermediate-acidic samples are andesites from Veria, dacites from Ag. Theodori, albitites, and granodiorites from Veria (Table 1).

Andesite has porphyritic texture and is characterized by the presence of sanidine phenocrysts (Figure 6a). It is rich in amphibole, clinopyroxene, and biotite phenocrysts set in a glassy to microcrystalline groundmass of flow texture. Plagioclase phenocrysts occur in all samples and are strongly zoned showing normal and oscillatory reverse zoning and they are partially to completely altered to sericite. Common accessory minerals include apatite, titanite, zircon, and magnetite. Dacite shows a porphyritic texture and is dominated by quartz, plagioclase (partially altered to sericite), hornblende, biotite, and sanidine (Figure 6b). However, the identification of clay minerals in rocks cannot be completed with great accuracy by petrographic examination. The accurate identification of clay minerals can be done after the clay fraction analysis, which does not constitute the goal of this paper and is quite difficult to be done for 63 aggregate rock samples.

The albitite presents granular texture with abundant idiomorphic albite and lesser quartz and clinopyroxene. Chlorite and epidote constitute secondary phases (Figure 6c). Accessory minerals include apatite, zircon, and Fe-oxides.

Granodiorite is characterized by the poikilitic texture and is composed of plagioclase, quartz, orthoclase, biotite, accessory apatite, titanite, and zircon (Figure 6d). Secondary minerals are epidote, chlorite, and sericite as an alteration product of plagioclase.

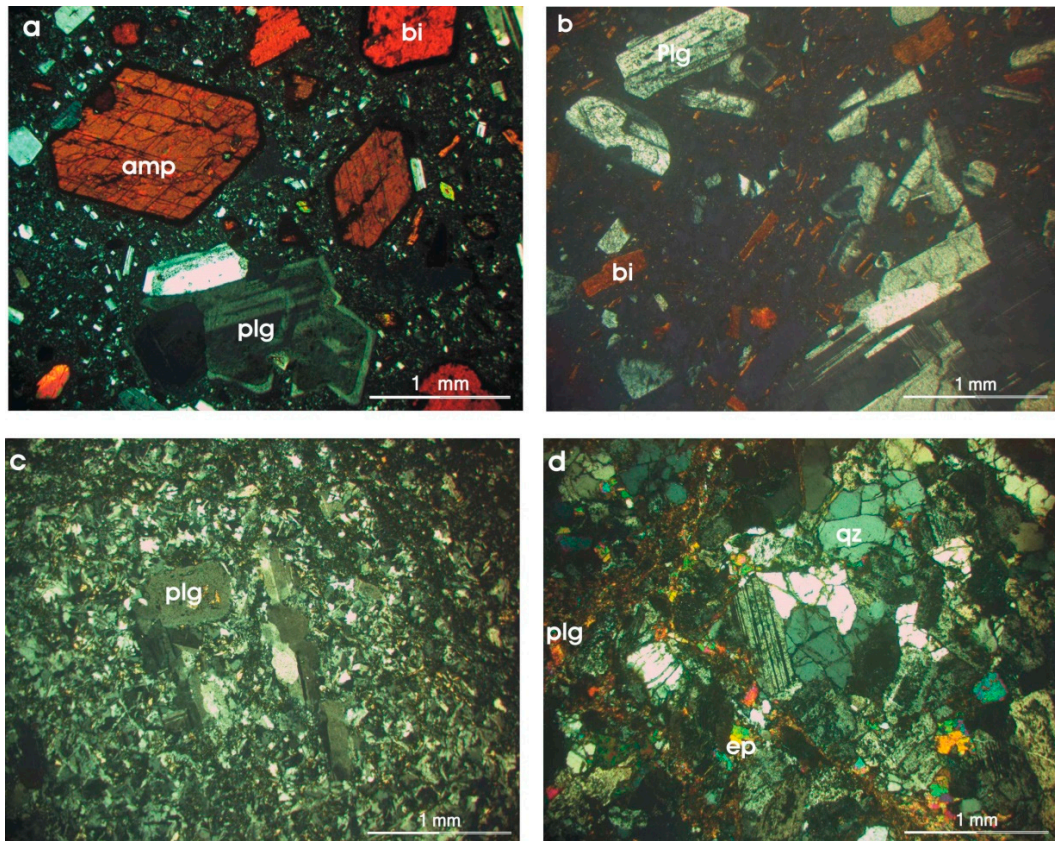


Figure 6. Photomicrographs of representative intermediate-acidic aggregate rocks (XPL): (a) phenocrysts of hornblende, biotite, and plagioclase in a porphyritic andesite (sample BE.81). (b) phenocrysts of plagioclase and lesser biotite in a porphyritic dacite (sample GE.23). (c) granular texture in albitite (sample BE.150). (d) granular texture of granodiorite with crystals of plagioclase, quartz, and secondary epidote (sample BE.139). Abbreviations: amp: amphibole, bi: biotite, plg: plagioclase, qz: quartz, ep: epidote.

Additionally, X-ray diffraction analysis showed that the mainly secondary minerals of the studied intermediate-acidic rocks are chlorite, epidote, and micas (Figure 7).

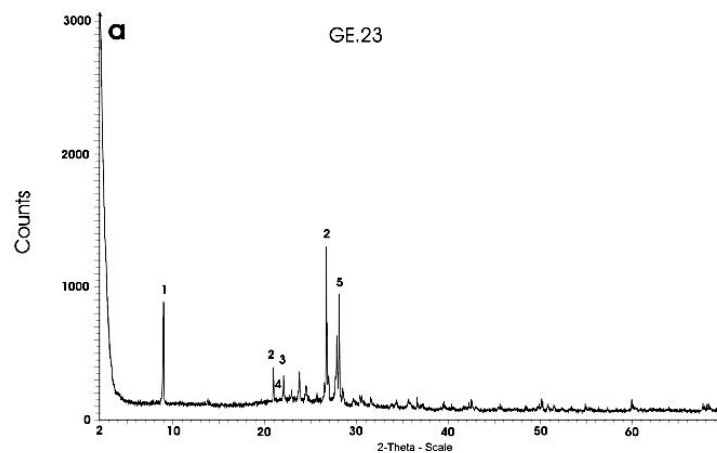


Figure 7. Cont.

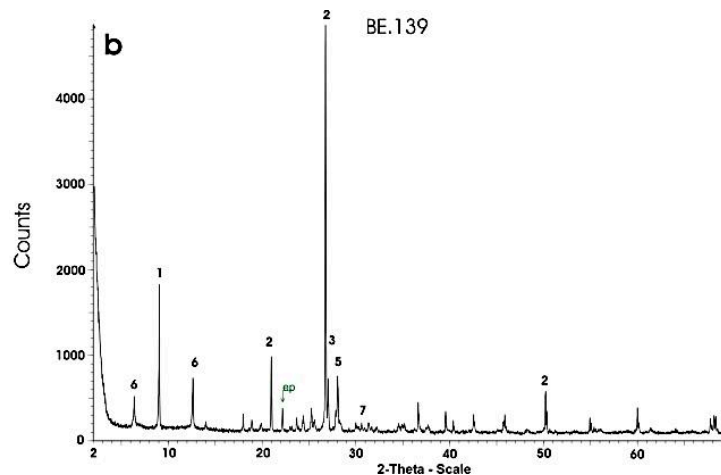


Figure 7. Representative X-ray diffraction patterns of the studied intermediate-acidic rock samples: (a) dacite and (b) granodiorite. Sample numbers are indicated as insets (1: mica, 2: quartz, 3: K-feldspars, 4: cristobalite, 5: plagioclase, 6: chlorite, 7: epidote).

4.2. Engineering Properties

The determined values of the engineering properties of the studied igneous rocks are listed in Table 2. Regarding the physical properties, the moisture content (w) ranges from 0.04% to 2.91% in the ultramafic rocks with the most serpentinized samples to present the highest values. The w of the studied mafic rocks ranges from 0.12% to 0.64% with the less altered ones displaying lower values. Researchers investigating ultramafic rocks observed similar ranges of moisture content [7,11,12]. The intermediate-acidic rocks present w values ranging from 0.27% to 2.70%. The values of total porosity (n_t) of the studied ultramafic rocks range from 0.16% to 6.81% while, for the mafic rocks, from 0.22% to 1.74%. For the intermediate-acidic rocks, the distribution of the n_t test results was substantially wide and ranged from 0.29% to 11.93% where sample GE.22 (dacite) appeared as the one with the highest ability to adsorb and restrain water. Concerning the dry density values of the studied igneous rocks, they vary within a narrow range from 19.02 to 35.41 KN/m³.

Regarding the geometrical properties observed in Table 2, the I_F values of the collected samples range between 12.00% and 85.96% with the most serpentinized harzburgite from the Gerania ophiolite complex showing the highest I_F value. The I_E values of the collected samples range between 9.80% and 73.65% with the most serpentinized harzburgite from the Gerania ophiolite complex showing the highest I_E value.

The mechanical properties of the collected igneous rocks were determined by the laboratory tests mentioned in Table 2. The Los Angeles abrasion (LA) results indicate that the altered volcanic samples have the highest abrasion loss. The uniaxial compressive strength values (UCS) range between 20.00 and 165.87 MPa with the diabase and albitite rocks having the highest strength. The indirect test for the measurement of the compressive strength (point load index) displays values that vary from 1.00 to 16.38 MPa with diabase, gabbro, and albitite showing the highest strengths. The Schmidt hammer values (SHV) of the collected samples, which vary from 26.40 to 62.40, indicate that the albitite rocks have the highest mechanical strength. Similar ranges of the mechanical properties have been reported by several researchers investigating similar lithologies [7,11,12].

The physicochemical parameters of the collected samples were determined by the soundness test and the methylene blue test (Table 2). The distribution of the soundness test (S) results obtained is substantially wide and ranges from 1.30% to 89.50%. Gabbro appeared as the most resistant in excessive volume changes. The methylene blue values of the studied samples range from 4.00 to 17.00 g/kg with the highly altered volcanic and ultramafic rocks containing the highest values. More specifically, in the intermediate-acidic volcanic rocks, the high values of MB_F are due to the high content of sericite, which potentially lead to swelling clay minerals.

Table 2. Results of the engineering properties of the studied aggregates.

No.	Sample Code/Locality	Physical Properties			Geometrical Properties		Mechanical Properties				Physicochemical Properties		
		w	n _t	ρ _d	I _F	I _E	LA	UCS	I _{s(50)}	SHV	S	MB _F	LOI
1	GE.4/Gerania	2.91	6.81	23.16	85.96	73.65	34.01	48.00	1.00	42.30	27.81	11.60	17.2
2	GE.17/Gerania	0.90	1.56	25.6	23.44	27.33	20.30	93.05	3.46	50.20	14.62	9.60	14.1
3	GE.25/Gerania	0.04	0.78	31.87	22.54	34.17	15.89	79.00	6.92	50.70	17.49	4.20	0.7
4	GE.26/Gerania	0.40	0.91	27.47	33.90	32.33	19.63	66.00	7.30	50.30	9.73	6.30	8.7
5	GE.28/Gerania	0.08	0.42	29.15	32.07	26.90	15.73	86.20	2.28	51.10	11.76	8.30	5.5
6	GE.30/Gerania	0.25	0.92	29.09	26.84	34.16	16.61	75.00	3.84	53.00	12.33	4.00	0.1
7	GE.31/Gerania	0.22	0.53	29.22	26.10	38.06	27.16	111.63	8.84	49.20	18.06	5.00	2.7
8	GE.32/Gerania	0.16	0.89	30.58	15.08	29.13	22.01	97.00	2.93	50.10	14.39	5.00	4.1
9	GE.33/Gerania	0.08	0.16	30.88	16.25	30.76	20.92	69.12	8.45	47.10	14.37	6.60	0.1
10	GE.34/Gerania	0.36	0.76	29.23	31.12	33.61	17.51	88.86	5.38	48.40	13.45	6.30	5.8
11	GE.35/Gerania	0.26	0.69	30.65	25.15	24.51	23.95	76.00	4.99	46.30	17.55	5.60	3.4
12	GE.36/Gerania	0.13	0.54	31.32	22.10	38.25	23.29	50.00	1.15	47.80	6.83	6.30	1.6
13	GE.37/Gerania	0.43	0.76	28.09	40.07	41.36	17.36	112.10	4.22	50.90	22.82	8.00	11.4
14	GE.39/Gerania	0.25	0.89	30.15	32.49	34.28	19.76	95.39	4.61	49.50	18.02	6.60	4.1
15	BE.01A/Veria	1.50	4.00	23.50	42.10	28.00	27.00	76.00	3.76	52.00	40.00	17.00	14.6
16	BE.01B/Veria	2.58	6.49	23.40	40.00	45.00	32.00	51.00	2.76	50.00	75.34	15.50	14.5
17	BE.12/Veria	2.18	3.40	24.00	37.20	21.00	23.00	55.40	1.88	50.00	26.00	13.32	13.5
18	BE.12B/Veria	2.20	3.30	23.50	35.00	20.00	25.16	55.40	1.88	52.00	25.20	12.80	13.4
19	BE.67/Veria	0.41	1.18	35.41	19.00	16.50	14.22	85.70	11.26	57.60	12.90	4.66	1.2
20	BE.103/Veria	1.95	5.00	24.66	34.50	35.00	28.98	32.00	1.16	49.00	74.00	9.33	14.2
21	BE.103B/Veria	1.94	4.99	25.00	33.00	30.00	28.97	32.00	1.10	48.00	75.12	9.00	14.1
22	BE.103C/Veria	1.94	4.99	24.00	30.00	33.00	28.97	39.00	1.30	49.00	70.00	8.35	14.1
23	BE.122/Veria	1.25	3.21	24.95	19.98	30.65	25.51	25.45	3.00	51.20	30.00	8.33	15.3
24	BE.122B/Veria	1.25	3.21	25.00	19.00	45.00	25.50	34.00	2.80	49.00	52.00	8.00	15.4
25	BE.133/Veria	1.40	2.80	25.06	16.12	35.00	22.50	35.00	1.55	50.00	36.46	10.00	13.4
26	ED.59/Edessa	1.52	6.29	24.32	26.49	49.00	40.36	20.00	1.35	47.00	75.00	12.00	14.1
27	ED.115/Edessa	2.10	4.53	23.12	33.62	38.00	20.77	28.00	1.94	50.00	65.00	10.00	14.4
28	BE.77/Veria	0.38	0.80	26.29	19.90	24.30	12.42	95.00	6.21	55.00	3.73	10.00	2.0
29	ED.93/Edessa	0.50	1.27	24.31	27.34	22.18	11.81	100.00	4.10	54.00	13.64	13.30	3.1
30	ED.94/Edessa	0.64	2.27	26.44	37.49	20.00	18.40	85.00	6.00	54.00	30.00	9.33	2.5
31	GE.24/Gerania	0.28	0.73	27.92	16.19	27.70	9.65	141.00	8.45	48.80	15.71	5.20	10.5
32	KIL.1/Guevgueli	0.22	1.32	29.17	12.14	47.47	16.59	99.33	6.79	50.30	3.76	5.60	1.5
33	KIL.4/Guevgueli	0.20	1.25	28.61	15.27	30.75	14.89	106.56	4.98	55.30	1.54	4.10	1.6

Table 2. Cont.

No.	Sample Code/Locality	Physical Properties			Geometrical Properties		Mechanical Properties				Physicochemical Properties		
		w	n _t	ρ _d	I _F	I _E	LA	UCS	I _{s(50)}	SHV	S	MB _F	LOI
34	KIL.5/Guevgueli	0.12	1.17	28.88	29.27	29.52	13.20	109.26	6.34	53.70	7.59	5.60	1.2
35	KIL.6/Guevgueli	0.12	0.54	28.73	23.33	39.79	12.50	112.67	13.50	51.10	6.37	5.00	0.9
36	KIL.9/Guevgueli	0.23	0.65	28.94	24.47	51.74	9.34	107.16	10.88	51.90	4.70	5.00	1.8
37	KIL.10/Guevgueli	0.19	0.67	30.08	18.43	22.64	12.58	108.36	7.70	51.10	8.44	5.60	1.6
38	BE.100/Veria	0.47	0.88	25.63	12.05	22.97	13.88	65.00	3.72	54.00	1.30	15.00	5.1
39	ED.26B/Edessa	0.60	1.74	27.19	13.62	23.90	20.68	80.00	5.22	55.00	6.54	13.33	5.8
40	KIL.2/Guevgueli	0.20	0.66	28.80	31.67	34.73	9.31	122.34	7.25	51.50	3.71	5.30	3.0
41	KIL.3/Guevgueli	0.14	0.48	28.35	36.91	44.77	10.77	126.72	11.33	55.20	2.52	6.50	2.2
42	KIL.8/Guevgueli	0.17	0.36	28.83	25.24	33.01	9.53	87.29	16.38	51.00	1.54	6.60	0.8
43	BE.24/Veria	0.44	0.70	27.69	33.30	9.80	11.34	124.57	9.03	57.20	3.45	9.95	2.2
44	BE.43/Veria	0.25	0.53	26.57	31.30	16.60	8.72	150.00	12.80	55.80	4.74	4.97	1.7
45	ED.24/Edessa	0.52	0.84	25.40	15.79	19.68	14.15	91.33	9.70	55.00	3.58	11.66	5.4
46	BE.113/Veria	0.42	0.45	25.30	24.05	14.00	7.39	97.15	9.70	57.00	2.02	10.00	3.2
47	ED.45/Edessa	0.41	0.24	26.66	29.93	16.00	9.99	110.00	8.40	56.00	3.12	11.66	6.0
48	ED.66B/Edessa	0.50	0.22	27.75	46.17	17.00	8.18	119.00	6.00	54.00	2.47	6.66	2.7
49	ED.110/Edessa	0.20	0.86	27.36	24.88	17.80	7.31	148.00	12.00	59.00	3.96	6.00	2.0
50	BE.15/Veria	0.29	0.13	25.99	56.10	12.70	10.54	165.87	12.63	62.00	8.68	5.32	3.0
51	ED.66A/Edessa	0.46	0.38	27.27	27.00	15.00	7.65	73.00	5.59	52.00	3.50	5.66	2.6
52	GE.22/Ag. Theodori	1.47	11.93	21.37	12.00	22.04	58.04	25.00	2.30	26.40	61.30	11.60	3.6
53	GE.23/Ag. Theodori	2.13	8.40	19.02	12.52	26.20	50.62	33.11	2.69	30.30	10.37	9.80	3.4
54	BE.81B/Veria	0.90	10.15	22.51	15.42	20.34	23.98	45.00	2.26	49.00	77.50	5.30	1.6
55	BE.82B/Veria	1.14	10.76	22.25	16.91	32.00	35.00	35.62	1.77	49.00	70.00	16.60	2.0
56	BE.88/Veria	1.38	2.84	23.94	10.87	20.04	18.36	53.00	4.50	53.00	39.00	10.98	1.6
57	BE.89/Veria	1.02	6.83	23.75	18.84	20.63	23.98	45.00	2.71	50.00	38.00	6.60	1.5
58	BE.101B/Veria	2.70	11.62	22.10	14.06	48.00	55.00	37.47	1.12	46.00	89.50	8.30	1.7
59	BE.139/Veria	0.60	1.70	27.00	18.68	16.00	7.71	91.00	3.68	54.40	2.41	6.33	2.4
60	BE.140/Veria	0.29	1.60	27.60	38.38	20.97	13.67	75.00	7.76	53.00	14.68	5.00	2.6
61	BE.149/Veria	0.35	0.97	25.23	32.67	18.95	10.25	70.00	5.43	51.00	21.00	6.66	2.5
62	BE.108/Veria	0.29	0.31	26.96	36.90	18.00	13.05	140.00	5.00	61.00	14.00	5.00	0.4
63	BE.150/Veria	0.27	0.29	26.93	37.96	14.89	11.00	145.00	10.00	62.40	14.80	5.30	0.4

(w = moisture content (%), n_t = total porosity (%), ρ_d = dry density (KN/m³), I_F = flakiness index (%), I_E = elongation index (%), LA = Los Angeles abrasion (%), UCS = uniaxial compressive strength (MPa), I_{s(50)} = point load index (MPa), SHV = Schmidt hammer value, S = soundness test (%), MB_F = methylene blue test (g/kg), LOI = Loss on Ignition (%)).

4.3. Factor Analysis

Factor analysis constitutes a multivariate statistical method occurring in various scientific fields [67]. An R-type factor analysis was performed including 12 engineering parameters by using IBM SPSS Statistics software.

The model that best fit to the analytical data is the triple-factor model based on the cumulative percentage variability and the higher communalities as well as the acquisition of geological and engineering statistically significant information. The factor axes were rotated based on the varimax orthogonal rotation method in order to accomplish the simplest possible model. The magnitude of each factor in each sample, i.e., the factor scores that define the influence of each factor in each sample was also taken into account when evaluating the results.

In the R-mode factor analysis, the first three factors account for ~76% of the total variance of the engineering parameters (Table 3). Communality displays the percentage of variance of a given parameter explicated by the sum of the factors. The higher communality obtained along with the determinant and KMO (Kaiser-Meyer-Olkin) values that are ≤ 0.0001 and ≥ 0.7 suggest that the three-factor model is statistically significant for all of the engineering properties, which permit the interpretation of the possible interrelations between these parameters of the studied lithotypes.

Table 3. R-mode factor analysis: eigenvalues, percentage, and cumulative percentage.

Factor	Initial Eigenvalues			Rotation Sums of Squared Loadings		
	Eigenvalue	Percentage of Variance (%)	Cumulative Percentage of Variance (%)	Eigenvalue	Percentage of Variance (%)	Cumulative Percentage of Variance (%)
1	6.328	52.732	52.732	4.302	35.849	35.849
2	1.576	13.135	65.867	3.204	26.697	62.546
3	1.257	10.472	76.338	1.655	13.792	76.338
4	0.737	6.140	82.479			
5	0.576	4.802	87.280			
6	0.464	3.868	91.148			
7	0.332	2.763	93.911			
8	0.248	2.069	95.980			
9	0.209	1.740	97.721			
10	0.146	1.214	98.935			
11	0.072	0.602	99.537			
12	0.056	0.463	100.000			

As shown in Table 4, the high communalities suggest that the 3-factor model is statistically significant, which indicates the interrelations between the engineering properties of the investigated igneous rocks used as aggregates. The first as well as the second factor are presented as bipolar and account for ~36% and ~27% of the total variance in addition to the third one, which displays only a positive pole and accounts for ~14% of the total variance. Moreover, the correlation coefficients (r) between the engineering parameters are presented in Table 5. Lastly, the amount of each factor in each sample (factor scores) was calculated. To compute the factor score for a given case for a given factor, each standardized variable score is multiplied by the corresponding standardized scoring coefficient. These products are described in Table 6.

Table 4. R-mode factor analysis: Loadings for the varimax rotated 3-factor model.

Variable	Factor 1	Factor 2	Factor 3	Communalities
w	0.538	0.685	0.352	0.882
n _t	0.749	0.520	-0.081	0.838
LA	0.862	0.346	0.016	0.863
UCS	-0.767	-0.420	-0.027	0.766
q _d	-0.332	-0.822	-0.006	0.787
S	0.650	0.505	0.134	0.696
MB _F	0.111	0.815	0.103	0.688
I _F	-0.275	0.119	0.808	0.743
I _E	0.585	-0.273	0.634	0.819
I _{S(50)}	-0.602	-0.474	-0.143	0.608
SHV	-0.856	-0.049	0.040	0.736
LOI	0.248	0.505	0.646	0.735

Table 5. Correlation coefficients (r) between the engineering properties.

	w	n _t	LA	UCS	ρ _d	S	MB _F	I _F	I _E	I _{S(50)}	SHV	LOI
w	1.000	0.750	0.718	−0.696	−0.756	0.735	0.587	0.221	0.337	−0.638	−0.463	0.680
n _t		1.000	0.853	−0.695	−0.738	0.811	0.433	−0.100	0.258	−0.587	−0.636	0.274
LA			1.000	−0.717	−0.570	0.711	0.401	−0.110	0.389	−0.623	−0.785	0.352
UCS				1.000	0.508	−0.698	−0.448	0.192	−0.326	0.736	0.629	−0.481
ρ _d					1.000	−0.584	−0.631	−0.067	−0.027	0.489	0.383	−0.430
S						1.000	0.373	−0.009	0.311	−0.615	−0.403	0.488
MB _F							1.000	0.065	0.037	−0.432	−0.189	0.501
I _F								1.000	0.214	0.023	0.174	0.332
I _E									1.000	−0.251	−0.387	0.374
I _{S(50)}										1.000	0.475	−0.521
SHV											1.000	−0.236
LOI												1.000

A Determinant = 1.73×10^{-9} , $r \leq 0.2$ adequate correlation. $r = 0.2$ to 0.4 weak correlation. $r = 0.4$ to 0.6 moderate correlation. $r = 0.6$ to 0.8 high correlation and $r \geq 0.8$ excessive correlation [32].

Table 6. R-mode factor analysis: factor scores of the 3-factor model.

Sample	Factor 1	Factor 2	Factor 3	Sample	Factor 1	Factor 2	Factor 3
GE.4	1.21	0.17	4.84	BE.81B	1.13	0.69	−1.62
GE.17	−0.21	0.51	0.39	BE.82B	1.05	1.70	−1.27
GE.22	2.93	0.72	−2.11	BE.88	−0.05	1.09	−1.35
GE.23	2.23	0.70	−1.66	BE.89	0.66	0.53	−1.27
GE.24	−0.31	−0.69	−0.01	BE.100	−0.67	1.04	−0.95
GE.25	0.45	−1.67	−0.16	BE.101B	2.68	0.45	−0.63
GE.26	0.03	−0.57	0.64	ED.24	−0.96	0.73	−0.84
GE.28	−0.21	−0.39	0.24	ED.26B	−0.49	0.69	−0.76
GE.30	0.29	−1.18	−0.05	ED.45	−1.44	0.79	−0.20
GE.31	0.45	−1.44	0.19	ED.94	−0.58	0.49	−0.09
GE.32	0.48	−1.15	−0.47	ED.59	1.63	0.57	0.93
GE.33	0.57	−1.39	−0.71	BE.103	0.87	0.89	1.04
GE.34	0.20	−0.94	0.47	BE.103B	0.86	0.93	0.78
GE.35	0.52	−1.07	−0.32	BE.103C	0.86	0.88	0.75
GE.36	0.97	−1.50	−0.06	BE.108	−1.26	0.02	−0.05
GE.37	−0.12	−0.54	1.56	BE.113	−1.40	0.77	−0.77
GE.39	0.23	−1.03	0.46	BE.122	0.50	0.56	0.31
KIL.1	0.64	−1.64	−0.14	BE.122B	1.06	0.04	0.81
KIL.2	−0.32	−1.07	0.43	BE.133	0.60	0.58	0.23
KIL.3	−0.54	−1.19	0.97	BE.139	−0.61	0.13	−0.92
KIL.4	−0.06	−0.98	−0.55	BE.140	−0.44	−0.38	0.03
KIL.5	−0.32	−0.84	−0.04	BE.149	−0.45	0.15	−0.35
KIL.6	−0.07	−1.51	0.04	ED.66B	−1.19	0.01	0.43
KIL.8	−0.38	−1.15	−0.17	ED.66A	−0.59	−0.10	−0.59
KIL.9	0.18	−1.78	0.65	ED.93	−0.97	1.08	−0.43
KIL.10	−0.22	−0.89	−0.69	ED.110	−1.42	−0.13	−0.53
BE.01	−0.57	2.01	1.07	ED.115	0.57	1.11	1.15
BE.01B	0.61	1.64	1.62	BE.150	−1.64	0.12	−0.12
BE.12	−0.34	1.79	0.69				
BE.12B	−0.40	1.87	0.56				
BE.15	−2.20	0.34	0.75				
BE.24	−1.56	0.63	−0.49				
BE.43	−1.33	−0.23	−0.35				
BE.67	−0.41	−1.21	−0.70				
BE.77	−0.70	0.25	−0.66				

5. Discussion

The study of the engineering parameters of rocks is of special significance since they are extensively used in many engineering projects. Relationships between mechanical properties have been reported by Ugur et al. [26], Kahraman [25], Petrounias et al. [11], Kazi and Al Mansour [22], and Al-Harathi et al. [1] investigating various igneous, sedimentary, and metamorphic aggregate rocks. A number of researchers such as Christensen [24] and Petrounias et al. [11] have also stated interrelationships between physical and mechanical properties. Moreover, several scientists have suggested negative correlations between the total porosity and the dry density (ρ_d) [68–72]. In addition,

numerous other researchers have interpreted the behavior of mechanical parameters in relation to their petrographic characteristics. Fortes et al. [73] stated that mineralogy combined with the textural and physical characteristics such as porosity and moisture content are modulatory factors for the mechanical behavior of aggregate rocks. Sabatakakis et al. [74] have shown a direct influence of microstructure on the strength of various sedimentary and igneous rocks. Numerous scientists have studied the impact of primary or secondary minerals contained in a variety of lithologies on their physical, mechanical, and physicochemical properties [6,11,12,75–79]. In this paper, the interrelationship between the engineering parameters was identified by using factor analysis based on the petrographic characteristics of the tested igneous rocks used as aggregates.

The R-mode factor analysis suggested a three-factor model for expressing the interrelations of the investigated parameters. The three factors reflect the three different strong trends among groups of interrelated parameters. The differences of the parameters are associated with differences of the petrographic characteristics of the studied rocks.

The poles of the engineering properties of the first factor (~36% of the total variance) are inversely correlated. The positive pole contains high loadings for LA abrasion, moderate loadings for n_t and S, and weaker loadings for w and I_E , which indicates that, with the increase of n_t , w , I_E of the investigated igneous rocks, their resistance in abrasion (LA) decreases. Additionally, the decrease of the resistance in excessive volume changes (S) is related to the increase of n_t , w , I_E of the investigated igneous rocks. The positive pole overall highlights the strong interrelation between the resistances of the investigated rocks in abrasion (LA) with their total porosity (n_t). There are several researchers who have associated physical properties such as n_t with the petrographic characteristics of the aggregate materials [11,12,80]. Generally, in Table 5, high correlations have been depicted between physical and mechanical properties such as n_t and LA, w and UCS, and n_t and UCS. These high correlations are due to the wide range of the engineering property results of the studied samples depending on their variable petrographic characteristics, which is shown in Table 2. The secondary phyllosilicate minerals (i.e., serpentine, chlorite, clay minerals) seem to be the dominant minerals influencing the engineering properties of igneous rocks used as aggregates [11]. Serpentine is the dominant secondary mineral in the studied ultramafic rock samples, which has been observed by the microscopic study, and it seems to determine n_t as well as w and S. Rocks with a high content of serpentine such as BE.01 (Figure 2b) was presented as more capable to incorporate water in their structure because of the ability of serpentine to form foliated masses contributing to the development of more porous areas, which result in higher values of n_t and in higher values of w in contrast to less serpentinized ultramafic rocks such as GE.34, GE.30, and BE.67 (Figure 2a,c,d). Furthermore, the existence of the mesh texture of serpentine creates weak planes, which allow hydrous solutions ($MgSO_4$) to flow along them. Subsequent crystallization and expansion of the salts cause failures of the rock structures [12], which highlights the strong interrelation of n_t with S. Chlorite. This is the dominant alteration product of the mafic rocks and significantly influences their total porosity. Rocks with high contents of chlorite such as ED.66A (Figure 4d) are considered more capable to incorporate water in their structure due to the platy and tabular structure of chlorite contained. This acts in similar ways to serpentine and results in higher values of n_t , w , S, and, consequently, LA abrasion in contrast to rocks such as KIL.5 and KIL.3 with less to minor chlorite contained [11]. The intermediate-acidic rocks present big differences in their engineering properties. Both albitite and granodiorite are plutonic and, therefore, quite compact rocks present mainly a granular texture responsible for their good cohesion and low porosity (Figure 6c,d) (BE.139, BE.150), which results in low n_t values and, subsequently, contributes on their low LA abrasion values. Dacites and andesites include many altered phenocrysts of plagioclase, which commonly transform to clay minerals and particularly in swelling clay minerals. These minerals, even in low percentages, are capable of adsorbing water in their phyllosilicate structure, which results in the increase of n_t and secondarily of w [11]. Samples BE.82B, BE.101B, and GE.22 potentially contain a low amount of swelling clay minerals presenting higher n_t values compared to the other volcanic rocks, which contributes to the decrease of their resistance in abrasion (LA).

The negative pole shows strong negative loadings for SHV and moderate loadings for UCS and $Is_{(50)}$, which indicates that these three different mechanical tests reflect the mechanical strength of rocks and present positive trends among them, which can be seen from Table 5. The relationship between SHV with UCS and $Is_{(50)}$ as well as the relation between the last two parameters are positive due to the similar nature of these mechanical tests. Sabatakakis et al. [81] and Giannakopoulou et al. [9] have also reported similar pairs of relationships. In addition, they are in accordance with Rigopoulos et al. [42] who examine various ophiolitic rocks. UCS is negatively related with LA abrasion since the presence of phyllosilicate minerals may create artificial surfaces of a weakness that results in the decrease of UCS and the increase of LA abrasion values simultaneously (i.e., serpentine and chlorite in ultramafic and mafic rocks, respectively) (Table 5). The petrographic study verifies the above relation as the most altered (ED.59, ED.26B) ultramafic and mafic samples presenting lower UCS values and lower resistance in abrasion in contrast to less altered ones (GE.34, ED.93). This interrelation is in accordance with Kazi and Mansour [22], Kahraman [25], and Ugur et al. [26]. Furthermore, physical properties such as w and n_t seems to influence negatively UCS [11,24] (Table 5). Regarding the intermediate-acidic rocks, they present a great variety in their mechanical properties (Table 2) due to their variable petrographic features. More specifically, this range is due to the further discrimination of this lithological group into plutonic and volcanic rocks as well as the different textures contained in these rocks. The porphyritic texture of the volcanic rocks seems to influence negatively on the mechanical behavior of the tested samples in contrast to the granular texture of the plutonic ones.

The second factor (~27% of the total data variability) is also bipolar and correlates physical, physicochemical, mechanical properties as well as LOI, which is considered to be an indirect index for the alteration degree of rocks expressed by the presence of serpentine in ultramafic rocks and by the presence of chlorite in mafic rocks [7]. Other researchers [7] have also cited similar ranges in LOI values to those of Table 2. More specifically, the positive pole of this factor displays high loadings for MB_F , moderate loadings for physical w , and weak loadings for n_t , S , LOI, which indicates that mineralogical components are the key parameters influencing the MB_F (GE.4, BE.01, BE.82B, and BE.88). This happens because swelling clay minerals can adsorb more water in their structure than other minerals. Similar conclusions have been cited in trachytes by Rigopoulos et al. [42]. The negative pole alike enhances the moderate relations between the physical and the mechanical properties such as q_d with UCS and $Is_{(50)}$ [2], which can be seen in Table 5 due to the wide range of these engineering properties (Table 2) relative to their various petrographic features.

The third factor has little effect on the engineering properties (~14% of the total variance). It presents only a positive pole correlating the studied geometrical properties with the LOI. More specifically, it shows high loadings for I_F and moderate loadings for I_E and LOI, which indicates that the flakiness and the elongation index increase in more altered rocks (BE.01B, BE.12, BE.103, and GE.26). Regarding the ultramafic rocks, these relationships attributed to the presence of serpentine, which belongs to the phyllosilicate subclass of minerals and promotes the production of flaky and elongated aggregate particles during the crushing process [27]. In mafic rocks, the presence of chlorite is responsible for the increase of I_F and I_E since it also belongs to the phyllosilicate subclass of minerals acting similarly to serpentine.

The first two factors together account for the ~63% of the total variance and, hence, the factor scores (Table 6) of the first factor plotted against the factor scores of the second one on a scatter diagram are shown in Figure 8. In this diagram, we can observe the engineering properties of the collected igneous aggregate rocks, which have been grouped into the positive and negative poles of factor 1 and factor 2. In order to give the best interpretation of the above relations, the diagram was divided into two clusters (A, B) of the samples while the samples display further differentiations.

In Figure 8, we can observe two groups of ultramafic rocks that present a clear gap between them and are detected in two clusters A and B. We also observe two groups of intermediate-acidic rocks divided into cluster A and B. The investigated mafic rock samples do not appear to have significant geological variation, which results in the two observed groups fitting within the same cluster (B).

More specifically, rocks detected in cluster A are the most serpentinized tested ultramafic rocks as well as the intermediate-acidic volcanic rocks (dacites and andesites), which display higher values of n_t , w , S , LA , I_E , MB_F , and LOI than those of cluster B. Giannakopoulou et al. [12] investigated the engineering properties of ultramafic rocks and have concluded that, with the increase of the serpentine percentage, n_t , w , LA , and S increased, respectively. Petrounias et al. [11] found similar conclusions regarding the relation between n_t and LA . Furthermore, samples of cluster A display lower values of q_d and of mechanical properties such as UCS , SHV , and $Is_{(50)}$ when compared with those of cluster B. For example, samples GE.30 and BE.67, which display a low percentage of serpentine (Figure 2c,d) have lower values of n_t , w , S , LA , and I_E and higher values of UCS , SHV , and $Is_{(50)}$ (Table 2). This is in contrast to sample BE.01, which is presented as more serpentinized (Figure 2b), and presents high values of n_t , w , S , LA , and I_E and lower values of the referred UCS , SHV , and $Is_{(50)}$ (Table 2). The plutonic intermediate-acidic rocks (granodiorite and albitite). These are detected in the B cluster presenting low values of n_t , w , S , and LA , and simultaneously high values of UCS , SHV , and $Is_{(50)}$ in contrast to the volcanic intermediate-acidic rock samples (dacites and andesites), which are detected in cluster A.

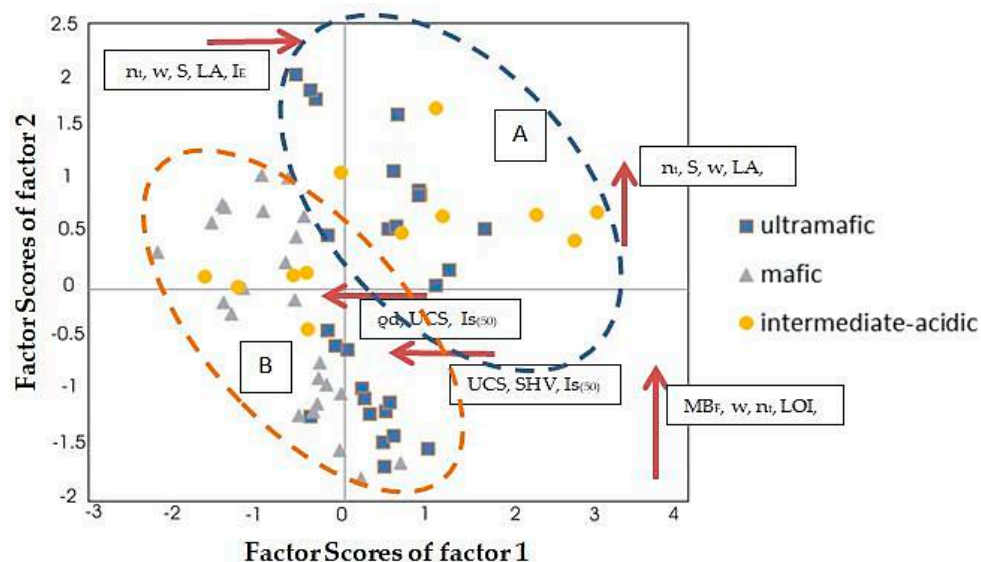


Figure 8. The factor scores of the first factor plotted against the factor scores of the second factor (R-mode factor analysis) were w = moisture content (%), n_t = total porosity (%), q_d = dry density (KN/m^3), I_E = elongation index (%), LA = Los Angeles abrasion (%), UCS = uniaxial compressive strength (MPa), $Is_{(50)}$ = point load index (MPa), SHV = Schmidt hammer value, S = soundness test (%), MB_F = methylene blue test (g/kg), and LOI = Loss on Ignition.

Rigopoulos et al. [42] proposed similar relationships between engineering parameters when investigating data of common lithologies. In this study, more representative rocks have been investigated such as in the number of lithological type indicating similar results to Rigopoulos et al. [42] and, simultaneously, presenting more statistically accurate conclusions about the engineering behavior of these types of rocks.

6. Conclusions

This paper focuses on the interrelations between the engineering properties of igneous rocks used as aggregate materials from various sources from Greece with the aid of the statistical method of factor analysis. R-mode factor analysis was used to correlate the engineering properties of the 63 rock samples. The 3-factor model, which accounts for 76% of the total variance of the original variables, better describes the interdependences between the physical, mechanical, geometrical, and physicochemical parameters of these igneous rocks. The referred engineering properties display

interrelationships, which is followed by changes of the petrographic characteristics of the tested aggregate rocks. These interrelationships have been depicted through the following factors. Factor 1, which is the most representative one (~36% of the total variance), shows interdependences between certain physical, mechanical, and physicochemical properties. Its positive pole reveals significant interdependence between n_t , w , S , LA , I_E , which indicates that, with the increase of n_t , w , and I_E of the investigated igneous rocks, their resistance in abrasion (LA) as well as their resistance in excessive volume changes (S) decrease, respectively. Moreover, the interdependence between UCS , SHV , and $Is_{(50)}$ is expressed in the negative pole of this factor. The presence of swelling minerals, which seems to determine the MB_F , present as a key parameter for the relations between w , n_t , and S , which has been depicted in Factor 2. Factor 3 (~14% of the total data variability) expresses the interdependence of I_F and I_E relative to their alteration (LOI). To conclude, this study has shown that factor analysis leads to a better understanding regarding how the engineering properties of igneous aggregate rocks change according to their petrographic characteristics.

Author Contributions: P.P.G. participated in the fieldwork, the elaboration of laboratory tests, the interpretation of the results, coordinated the research, and wrote the manuscript. P.P. participated in the fieldwork, the elaboration of laboratory tests, the interpretation of the results, and contributed to the manuscript writing. B.T. participated in the fieldwork and in the writing of the paper. S.K. performed the statistical analyses, assisted in the interpretation, and contributed to the manuscript writing. A.R. participated in the fieldwork and in the interpretation of the results. K.H. participated in the interpretation of the results and S.F.T. assisted in the evaluation of parts of data.

Funding: This research received no external funding.

Acknowledgments: We express our thanks to Spiros Sergiou for his assistance in the interpretation of the statistical results and the critical reviews from the anonymous reviewers that have improved our manuscript are gratefully acknowledged.

Conflicts of Interest: The authors declare no conflict of interest.

References

1. Al-Harathi, A.A.; Al-Amri, R.M.; Shehata, W.M. The porosity and engineering properties of vesicular basalt in Saudi Arabia. *Eng. Geol.* **1999**, *54*, 313–320. [[CrossRef](#)]
2. Turgul, A.; Zarif, I.H. Correlation of mineralogical and textural characteristics with engineering properties of selected granitic rocks from Turkey. *Eng. Geol.* **1999**, *51*, 303–317.
3. Smith, M.R.; Collis, L. *Aggregates: Sand, Gravel and Crushed Rock Aggregates for Construction Purposes*; Spec. Publ. 17; The Geological Society: London, UK, 2001.
4. Pomonis, P.; Rigopoulos, I.; Tsikouras, B.; Hatzipanagiotou, K. Relationships between petrographic and physico-mechanical properties of basic igneous rocks from the Pindos ophiolitic complex, NW Greece. *Bull. Geol. Soc. Greece* **2007**, *2*, 947–958. [[CrossRef](#)]
5. Rigopoulos, I.; Tsikouras, B.; Pomonis, P.; Hatzipanagiotou, K. The influence of alteration on the engineering properties of dolerites: The example from the Pindos and Vourinos ophiolites (northern Greece). *Int. J. Rock Mech. Min. Sci.* **2010**, *47*, 69–80. [[CrossRef](#)]
6. Yilmaz, N.G.; Goktan, R.M.; Kibici, Y. Relations between some quantitative petrographic characteristics and mechanical strength properties of granitic building stones. *Int. J. Rock Mech. Min. Sci.* **2011**, *48*, 506–513. [[CrossRef](#)]
7. Rigopoulos, I.; Tsikouras, B.; Pomonis, P.; Hatzipanagiotou, K. Assessment of the engineering behavior of ultramafic and mafic rocks using chemical indices. *Eng. Geol.* **2015**, *196*, 222–237. [[CrossRef](#)]
8. Petrounias, P.; Rogkala, A.; Kalpogiannaki, M.; Tsikouras, B.; Hatzipanagiotou, K. Comparative study of physico-mechanical properties of ultrabasic rocks (Veria-Naousa ophiolite) and andesites from central Macedonia (Greece). *Bull. Geol. Soc. Gr.* **2016**, *50*, 1989–1998.
9. Giannakopoulou, P.P.; Tsikouras, B.; Hatzipanagiotou, K. The interdependence of mechanical properties of ultramafic rocks from Gerania ophiolitic complex. *Bull. Geol. Soc. Gr.* **2016**, *50*, 1829–1837.
10. Petrounias, P.; Giannakopoulou, P.P.; Rogkala, A.; Stamatis, P.M.; Tsikouras, B.; Papoulis, D.; Lampropoulou, P.; Hatzipanagiotou, K. The Influence of Alteration of Aggregates on the Quality of the Concrete: A Case Study from Serpentinities and Andesites from Central Macedonia (North Greece). *Geosciences* **2018**, *8*, 115. [[CrossRef](#)]

11. Petrounias, P.; Giannakopoulou, P.P.; Rogkala, A.; Lampropoulou, P.; Koutsopoulou, E.; Papoulis, D.; Tsikouras, B.; Hatzipanagiotou, K. The Impact of Secondary Phyllosilicate Minerals on the Engineering Properties of Various Igneous Aggregates from Greece. *Minerals* **2018**, *8*, 329. [[CrossRef](#)]
12. Giannakopoulou, P.P.; Petrounias, P.; Rogkala, A.; Tsikouras, B.; Stamatis, P.M.; Pomonis, P.; Hatzipanagiotou, K. The influence of the mineralogical composition of ultramafic rocks on their engineering performance: A case study from the Veria-Naousa and Gerania ophiolite complexes (Greece). *Geosciences* **2018**, *8*, 251. [[CrossRef](#)]
13. Arel, E.; Turgul, A. Weathering and its relation to geomechanical properties of Gavusbasi granitic rocks in northwestern Turkey. *Bull. Eng. Geol. Environ.* **2001**, *60*, 123–133.
14. Ceryan, S.; Tudes, S.; Ceryan, N. Influence of weathering on the engineering properties of Harsit granitic rocks (NE Turkey). *Bull. Eng. Geol. Environ.* **2008**, *67*, 97–104. [[CrossRef](#)]
15. Das, A.; Krishnaswami, S.; Sarin, M.M.; Pande, K. Chemical weathering in the Krishna Basin and Western Ghats of the Deccan Traps, India: Rates of basalt weathering and their controls. *Geochim. Cosmochim. Acta* **2005**, *69*, 2067–2084. [[CrossRef](#)]
16. Orhan, M.; Isik, N.; Topal, T.; Ozer, M. Effect of weathering on the geomechanical properties of andesite, Ankara-Turkey. *Environ. Geol.* **2006**, *50*, 85–100. [[CrossRef](#)]
17. Cascini, L.; Nocera, S.; Critelli, S.; Gulla, G.; Matano, F. Weathering and land sliding in Sila Massif gneiss (Northern Calabria, Italy). In Proceedings of the 7th International Congress-International Association of Engineering Geology, Rotterdam, The Netherlands, 5–9 September 1994; pp. 1613–1622.
18. Price, J.R.; Velbel, M.A. Chemical weathering indices applied to weathering profiles developed on heterogeneous felsic metamorphic parent rocks. *Chem. Geol.* **2003**, *202*, 397–416. [[CrossRef](#)]
19. Augustin, N.; Lackschewitz, K.S.; Kuhn, T.; Devey, C.W. Mineralogical and chemical mass changes in mafic and ultramafic rocks from the Logatchev hydrothermal field (MAR 15°N). *Mar. Geol.* **2008**, *256*, 18–29. [[CrossRef](#)]
20. Rigopoulos, I.; Tsikouras, B.; Pomonis, P.; Hatzipanagiotou, K. The impact of petrographic characteristics on the engineering properties of ultrabasic rocks from northern and central Greece. *Q. J. Eng. Geol. Hydrogeol.* **2012**, *45*, 423–433. [[CrossRef](#)]
21. Undul, O.; Turgul, A. The influence of weathering on the engineering properties of dunites. *Rock Mech. Rock Eng.* **2012**, *45*, 225–239. [[CrossRef](#)]
22. Kazi, A.; Al-Mansour, Z.R. Influence of geological factors on abrasion and soundness characteristics of aggregates. *Eng. Geol.* **1980**, *15*, 195–203. [[CrossRef](#)]
23. Chargin, J.S.; Shakoor, A. Evaluation of empirical methods for measuring the uniaxial compressive strength. *Int. J. Rock Mech. Min. Sci.* **1990**, *27*, 495–503. [[CrossRef](#)]
24. Christensen, N.I. Serpentinities, peridotites and seismology. *Int. Geol. Rev.* **2004**, *46*, 795–816. [[CrossRef](#)]
25. Kahraman, S.; Fener, M. Predicting the Los Angeles abrasion loss of rock aggregates from the uniaxial compressive strength. *Mater. Lett.* **2007**, *61*, 4861–4865. [[CrossRef](#)]
26. Ugur, I.; Demirdag, S.; Yavuz, H. Effect of rock properties on the Los Angeles abrasion and impact test characteristics of the aggregates. *Mater. Charact.* **2010**, *61*, 90–96. [[CrossRef](#)]
27. Rigopoulos, I.; Tsikouras, B.; Pomonis, P.; Hatzipanagiotou, K. Correlations between petrographic and geometrical properties of ophiolitic aggregates from Greece. *Bull. Eng. Geol. Environ.* **2014**, *73*, 1–12. [[CrossRef](#)]
28. Joreskog, K.G.; Klovan, J.E.; Reyment, R.A. *Geological Factor Analysis*; Elsevier: Amsterdam, The Netherlands, 1976.
29. Temple, J.T. The use of factor analysis in geology. *Math. Geol.* **1978**, *10*, 379–387. [[CrossRef](#)]
30. Davis, J.C. *Statistics and Data Analysis in Geology*; Wiley & Sons: New York, NY, USA, 1986.
31. Schaeben, H. Geology and mathematics: Progressing mathematization of geology. *Geol. Rundsch.* **1988**, *77*, 591–607. [[CrossRef](#)]
32. Morrison, D.F. *Multivariate Statistical Methods*, 5th ed.; Duxbury Press: Pacific Grove, CA, USA, 2004.
33. Anazawa, K.; Ohmori, H. The hydrochemistry of surface waters in Andesitic Volcanic area, Norikura volcano, central Japan. *Chemosphere* **2005**, *59*, 605–615. [[CrossRef](#)]
34. Hitchon, B.; Billings, K.G.; Klovan, J.E. Geochemistry and origin of formation waters in the western Canada sedimentary basin, III. Factors controlling chemical composition. *Geochim. Cosmochim. Acta* **1971**, *35*, 567–598. [[CrossRef](#)]

35. Voudouris, K.S.; Lambrakis, N.J.; Papatheodorou, G.; Daskalaki, P. An application of factor analysis for the study of the hydrogeological conditions in Plio-Pleistocene aquifers of N.W Achaia (N.W Peloponnesus, Greece). *Math. Geol.* **1997**, *29*, 43–59. [[CrossRef](#)]
36. David, M.; Campiglio, C.; Darling, R. Progress in R- and Q-mode analysis. Correspondence analysis and its application to the study of geological processes. *Can. J. Earth Sci.* **1974**, *11*, 131–146. [[CrossRef](#)]
37. Kumru, M.N.; Bakac, M. R-mode factor analysis applied to the distribution of elements in soils from the Aydin basin, Turkey. *J. Geochem. Explor.* **2003**, *77*, 81–91. [[CrossRef](#)]
38. Meng, S.X.; Maynard, J.B. Use of statistical analysis to formulate conceptual models of geochemical behavior: Water chemical data from the Botucatu aquifer in Sao Paulo State, Brazil. *J. Hydrol.* **2001**, *250*, 78–97. [[CrossRef](#)]
39. Yidana, S.M.; Ophori, D.; banoeng-Yakubo, B. A multivariate statistical analysis of surface water chemistry data- the Ankobra Basin, Ghana. *J. Environ. Manag.* **2008**, *86*, 80–87. [[CrossRef](#)] [[PubMed](#)]
40. Hsu, L.C.; Huang, C.Y.; Chuang, Y.H.; Chen, H.W.; Chan, Y.T.; Teah, H.Y.; Chen, T.Y.; Chang, C.F.; Liu, Y.T.; Tzou, Y.M. Accumulation of heavy metals and trace elements in fluvial sediments received effluents from traditional and semiconductor industries. *Sci. Rep.* **2016**, *6*, 34250. [[CrossRef](#)] [[PubMed](#)]
41. Wiatr, I.; Stenzel, P. Application of factor analysis to classification of engineering-geological environments. *J. Int. Assoc. Math. Geol.* **1974**, *6*, 17–31. [[CrossRef](#)]
42. Rigopoulos, I.; Tsikouras, B.; Pomonis, P.; Hatzipanagiotou, K. Determination of the interrelations between the engineering parameters of construction aggregates from ophiolite complexes of Greece using factor analysis. *Constr. Build. Mater.* **2013**, *49*, 747–757. [[CrossRef](#)]
43. Rogkala, A.; Petrounias, P.; Tsikouras, B.; Hatzipanagiotou, K. New occurrence of pyroxenites in the Veria-Naousa ophiolite (north Greece): Implications on their origin and petrogenetic evolution. *Geosciences* **2017**, *7*, 92. [[CrossRef](#)]
44. Decourt, J.; Aubouin, J.; Savoyat, E. Le sillon mesohellenique et la zone pelagonienne. *Bull. Soc. Geol. Fr.* **1977**, *1*, 32–70.
45. Michailidis, K.M. Zoned chromites with high MN-contents in the Fe-Ni-Cr-laterite ore deposits from the Edessa area in Northern Greece. *Miner. Deposita* **1990**, *25*, 190–197. [[CrossRef](#)]
46. Pe-Piper, G.; Piper, D.J.W. *The Igneous Rocks of Greece; The Anatomy of an Orogen; Beitrge zur Regionalen Geologie der Erde (Series); Gebrder Borntraeger: Stuttgart, Germany, 2002; 573p.*
47. Clément, B. Evolution géodynamique d'un secteur des Hellénides internes: L'Attique-Béotie (Grèce continentale). Ph.D. Thesis, University Lille, Lille, France, 1983.
48. Vacondios, I. Etude metallogénique des chromites liées aux ophiolites de type Méditerranée occidentale ou orientale: Le chromites de Tinos et des Gerannes. Ph.D. Thesis, University of Patras, Patras, Greece, 1997.
49. Danelian, T.; Robertson, A.H.F. Palaeogeographic implications of the age of radiolarian-rich sediments in Beotia (Greece). *Bull. Geol. Soc. Greece* **1998**, *32*, 21–29.
50. Zachariadis, P.; Kostopoulos, D.; Reischmann, T.; Himmerkus, F.; Matukov, D.; Sergeev, S. U-Pb ion-microprobe zircon dating of subduction-related magmatism from northern Greece: The ages of the Guevgueli, Thessaloniki and Chalkidiki igneous complexes. *Geophys. Res. Abstr.* **2006**, *8*, 055560.
51. Saccani, E.; Bortolotti, V.; Marroni, M.; Pandolfi, L.; Photiades, A.; Principi, G. The Jurassic association of backarc basin ophiolites and calc-alkaline volcanics in the Guevgueli complex (Northern Greece): Implication for the evolution of the Vardar zone. *Ophioliti* **2008**, *33*, 209–227.
52. Boccaletti, M.; Manetti, P.; Peccerillo, A. The Balkanides as an Instance of Back-Arc Thrust Belt: Possible relation with the Hellinides. *Geol. Soc. Am. Bull.* **1974**, *85*, 1077–1084. [[CrossRef](#)]
53. Eleftheriadis, G.; Castorina, F.; Soldatos, T.; Masi, U. Geochemical and Sr-Nd isotopic evidence for the genesis of the Late Cainozoic Almopia volcanic rocks (Central Macedonia, Greece). *Min. Petrol.* **2003**, *78*, 21–36. [[CrossRef](#)]
54. Freyberg, B.V. *Geologie des Isthmus von Korinth. Erlanger Geologische Abhandlungen, 95*; Junge and Sohn, Universitäts-Buchdruckerei: Erlangen, Germany, 1973.
55. *Part 1: Composition, Specifications and Conformity Criteria for Common Cements*; EN 932-1; European Standard: Warsaw, Poland, 2011.
56. *Part 3: Procedure and Terminology for Simplified Petrographic Description*; EN 932; European Standard: Warsaw, Poland, 1996.

57. AASHTO T255. *Standard Method of Test for Total Evaporable Moisture Content of Aggregate by Drying*; ASTM International: West Conshohocken, PA, USA, 2000.
58. ISRM Suggested Methods. *Rock Characterization Testing and Monitoring*; Brown, E., Ed.; Pergamon Press: Oxford, NY, USA, 1981.
59. BS 812, *Testing Aggregates, Part 105: Methods for Determination of Particle Shape. Section: 105.1: Flakiness Index*; British Standards Institution: London, UK, 1989.
60. BS 812, *Testing Aggregates, Part 105: Methods for determination of particle Shape. Section: 105.2: Elongation Index*; British Standards Institution: London, UK, 1990.
61. ASTM C-131. *Resistance to Abrasion of Small-Size Coarse Aggregate by Use of the Los Angeles Machine*; American Society for Testing and Materials: Philadelphia, PA, USA, 1989.
62. ASTM D-2938. *Standard Test Method of Unconfined Compressive Strength of Intact Rock Core Specimens*; Annual Book of Standards, 4.08; American Society for Testing and Materials: Philadelphia, PA, USA, 1986.
63. ISRM. Suggested method for determining point load strength. *Int. J. Rock Mech Min. Sci. Geomech. Abstr.* **1985**, *22*, 51–62. [[CrossRef](#)]
64. EN 1367-2. *Tests for Thermal and Weathering Properties of Aggregates—Part 2: Magnesium Sulfate Test*; European Committee for Standardization: Brussels, Belgium, 1999.
65. EN 933-9, *Tests for Geometrical Properties of Aggregates—Part 9: Assessment of Fines-Methylene Blue Tests*; European Committee for Standardization: Brussels, Belgium, 1998.
66. ASTM D 7348, *Standard Test Methods for Loss on Ignition (LOI) of Solid Combustion*; Residues, ASTM International: West Conshohocken, PA, USA, 2011.
67. Davis, J.H. *Statistics and Data Analysis in Geology*, 3rd ed.; Wiley & Sons: New York, NY, USA, 2002.
68. Dally, R.A.; Manger, G.E.; Clark, S.P. Density of rocks. In *Handbook of Physical Constants*; Geological Society of America: Boulder, CO, USA, 1966; Volume 97, pp. 19–26.
69. Ramana, Y.V.; Venkatanaryana, B. An air porosimeter for the porosity of rocks. *Int. J. Rock Mech. Min. Sci.* **1971**, *8*, 2953–2960. [[CrossRef](#)]
70. Tugrul, A.; Zarif, I.H. Engineering aspects of limestone weathering in Instabul, Turkey. *Bull. Eng. Geol. Environ.* **2000**, *58*, 191–206. [[CrossRef](#)]
71. Tugrul, A. The effect of weathering on pore geometry and compressive strength of selected rock types from Turkey. *Eng. Geol.* **2004**, *75*, 215–227. [[CrossRef](#)]
72. Koukis, G.; Sabatakakis, N.; Spyropoulos, A. Resistance variation of low-quality aggregates. *Bull. Eng. Geol. Environ.* **2007**, *66*, 457–466. [[CrossRef](#)]
73. Fortes, A.P.P.; Anastasio, S.; Kuznetsova, E.; Danielsen, S.W. Behaviour of crushed rock aggregates used in asphalt surface layer exposed to cold climate conditions. *Environ. Earth Sci.* **2016**, *75*, 1414. [[CrossRef](#)]
74. Sabatakakis, N.; Tsiambaos, G.; Ktena, S.; Bouboukas, S. The effect of microstructure on mi strength parameter variation of common rock types. *Bull. Eng. Geol. Environ.* **2017**, *77*, 1673–1688. [[CrossRef](#)]
75. Miskovsky, K.; Tabora, D.M.; Kou, S.Q.; Lindqvist, P.A. Influence of the mineralogical composition and textural properties on the quality of coarse aggregates. *J. Mater. Eng. Perform.* **2004**, *13*, 144–150. [[CrossRef](#)]
76. Zorlu, K.; Gokceoglu, C.; Ocakoglu, F.; Nefeslioglu, H.A.; Acikalın, S. Prediction of uniaxial compressive strength of sandstones using petrography-based models. *Eng. Geol.* **2008**, *96*, 141–158. [[CrossRef](#)]
77. Pola, A.; Crosta, G.; Fusi, N.; Barberini, V.; Norini, G. Influence of alteration on physical properties of volcanic rocks. *Tectonophysics* **2012**, *566–567*, 67–86. [[CrossRef](#)]
78. Frolova, J.; Ladygin, V.; Rychagov, S.; Zukhubaya, D. Effects of hydrothermal alterations on physical and mechanical properties of rocks in the Kuril-Kamchatka island arc. *Eng. Geol.* **2014**, *183*, 80–95.
79. Piasta, W.; Gora, J.; Turkiewicz, T. Properties and durability of coarse igneous rock aggregates and concretes. *Constr. Build. Mater.* **2016**, *126*, 119–129. [[CrossRef](#)]
80. Undul, O.; Turgul, A. On the variations of geo-engineering properties of dunites and diorites related to weathering. *Environ. Earth Sci.* **2016**, *75*, 1326. [[CrossRef](#)]
81. Sabatakakis, N.; Koukis, G.; Tsiambaos, G.; Papanakli, S. Index properties and strength variation controlled by microstructure for sedimentary rocks. *Eng. Geol.* **2008**, *97*, 80–90. [[CrossRef](#)]

